ELSEVIER

Cement & Concrete Composites 22 (2000) 243–251

Cement & Concrete Composites

www.elsevier.com/locate/cemconcomp

Micro-mechanical analysis of splitting failure in concrete reinforced with fiber reinforced plastic rods

J.Q. Ye *, Z.J. Wu

School of Civil Engineering, University of Leeds, Leeds LS2 9JT, UK

Abstract

The present investigation provides a micro-mechanical model for the splitting failure analysis of fiber reinforced plastic (FRP) reinforced concrete members subjected to longitudinal tensile stresses. The model consists of three co-axial cylinders: (a) the inner elastic FRP rod; (b) the mid cracked part of concrete; and (c) the outer elastic part of concrete. The anisotropic properties of reinforcement, the compatibility of longitudinal strain at interface and the effect of Poisson's ratio of concrete are taken into account in the analysis. The method can be used to predict the stress distributions in the hybrid structure and the relations between the growth of cracks and the applied end forces. It is found that the number of splitting cracks and the material properties of the anisotropic FRP rods are not the dominant factors in splitting failure. It is also observed that neglecting Poisson's ratio of cracked concrete may under-estimate stresses in the hybrid structure. © 2000 Elsevier Science Ltd. All rights reserved.

Keywords: Stress analysis; Composites; FRP/concrete hybrid structure; Splitting failure

1. Introduction

Fiber reinforced plastic (FRP) materials are under widespread investigation as improved concrete reinforcement by virtue of their promise of improved durability in comparison with conventional steel materials. These kinds of materials consist of continuous fibers of glass, aramid, or carbon embedded in a polymer resin matrix such as polyester, epoxy, or vinylester. The fibers are oriented at high volume fractions in the direction of significant stress. Properties of interest to designers offered by composites [1] are high tensile strength, high damping, low weight, high fatigue strength, corrosion immunity and electromagnetic neutrality. Over last few years, mass-produced FRP structural members, such as FRP rods, cast with conventional concrete [2], were introduced into civil engineering structures including buildings, bridges and other infrastructures [3]. The safety and reliability of these FRP/concrete hybrid structures, being the new kinds of engineering structures, are always concerned. It is known that under different loading conditions, a hybrid FRP/concrete member may fail in a number of possible ways. It may fracture under tensile loading and fail or buckle under shear or compressive stresses. Under bending moments, the structure may have flexural failure due to the action of normal stresses. In all these cases, bond failure may occur. Generally, the bond failure can be divided into two categories: (1) pull-out failure where either the interfacial shear stress between a FRP rod and surrounding concrete exceeds its shearing strength or the concrete around the reinforcement is crushed and the FRP rod is pulled out; and (2) splitting failure where the concrete cover splits by internal (radial) pressure and the mechanical interlocking is lost.

To study the bond and simulate the failure modes in FRP/concrete hybrid systems, extensive laboratory works have been done around the world in recent years [4]. One of the most commonly used methods to characterize the first bond failure is the direct pull-out test (Fig. 1), where a FRP rod which fully penetrates a block or cylinder of concrete is pulled out by direct tension while applied load as well as displacement at the loaded and/or free ends of the rod are recorded [5]. Some researchers have also measured longitudinal strain distribution either on or inside the rods at positions within the embedment length, which helps to characterize the load transfer between reinforcement and concrete during pull-out [6]. Based on the results obtained from these experiments it has been found that under adequate

* Corresponding author. Fax: +44-0113-2332265.
E-mail address: j.ye@leeds.ac.uk (J.Q. Ye).

PII: S0958-9465(00)00023-8

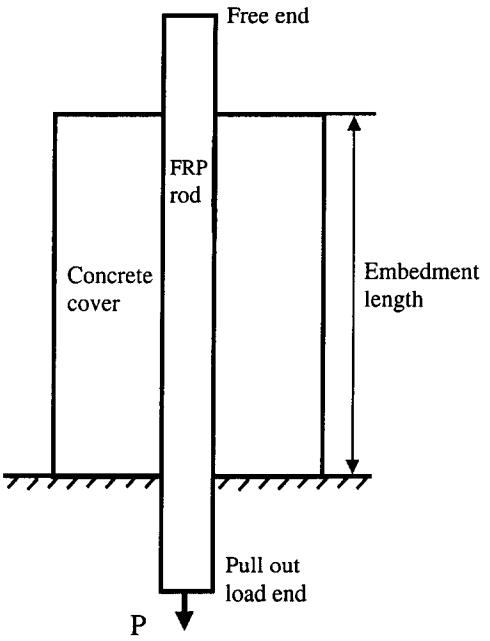

Fig. 1. Schematically shown of direct pull-out test.

concrete cover, FRP rods will undergo either tensile failure or bond slip depending on the length of embedment. However, in both cases, little or no damage to the concrete cover has been observed and, hence the properties of the FRP reinforcement is considered as a dominating factor in characterizing the first type of bond failure of FRP/concrete hybrid systems. The second type of bond failure mode occurs in some FRP/concrete hybrid structures, such as those with sand particle coatings and lugged FRP rods [4], subjected to longitudinal tensile forces. The failure mechanism of this type of structures depends on the design of the FRP rods. The mechanical interlock varies and may be as strong as that of steel reinforcement in typical concrete, where concrete failure occurs before debonding. Obviously, large compressive forces [7], due to the roughness of the interface and the incompatibility between the deformation of FRP rods and concrete, are transferred to concrete. These forces give rise to relevant stress components within concrete, which causes splitting failure of the hybrid structures. In practical FRP/concrete systems, both pull-out and splitting failures may happen, depending on the geometry of the structures, the design of the FRP rods, the applied forces and the constraints imposed on the hybrid structures.

The present paper only deals with the second type of bond failure, i.e., splitting failure [8], where the internal pressure is the main concern (The first type of bond failure has been dealt with separately [9].) The objectives of the present investigation are to provide a micro-mechanical analysis for the splitting failure of FRP/concrete hybrid structure under tensile stress. The new model (Fig. 4) is based on the one used by Olofsson et al. [10], Tepfers [11] and Cornelius [12] for steel reinforcement concrete and now includes anisotropic properties of reinforcement, the effect of Poisson's ratio of cracked concrete and the compatibility of longitudinal strains at interface. As a result, the present analysis can give the stress distribution around the bond area of the structures and establish the relationship between crack length and the applied tensile loads at the ends. Furthermore, this research is also an extension of the micro-mechanical models for describing the response of plain concrete [7] and the research on interfacial properties of composites [13]. The method developed is used to predict the stress distributions of a FRP reinforced element after the concrete around the FRP rod has cracked.

2. Splitting failure of FRP/concrete hybrid structures

2.1. Elastic analysis

When a FRP reinforced concrete structure is subjected to external loads, stress transfer occurs at the interface between FRP and concrete. To analyze the stress transfer, a representative volume element (RVE) model of the structure is often chosen. The model shown in Fig. 2 originates from concrete beams or plates reinforced with longitudinally parallel FRP rods under uniform tension (Fig. 3). This is also the case when a reinforced beam is subjected to bending. The RVE shown in Fig. 2 has been successfully used by many researchers [14,15]. In more details the RVE consists of a FRP rod of diameter d and a surrounding concrete cylinder of diameter D. The elastic analysis of the RVE is carried out under the cylindrical coordinates (r,θ,z). Assuming that the FRP rod is transversely isotropic while the concrete is isotropic, the elastic analyses of the model are based on following equations:

$$\begin{aligned}&\frac{\partial\sigma_r}{\partial r}+\frac{\sigma_r-\sigma_\theta}{r}+\frac{\partial\tau_{rz}}{\partial z}=0,\\&\frac{\partial\tau_{rz}}{\partial r}+\frac{\tau_{rz}}{r}+\frac{\partial\sigma_z}{\partial z}=0,\end{aligned}\tag{1}$$

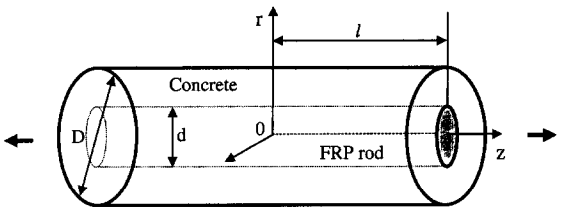

Fig. 2. RVE of FRP/concrete structure under tensile stress.

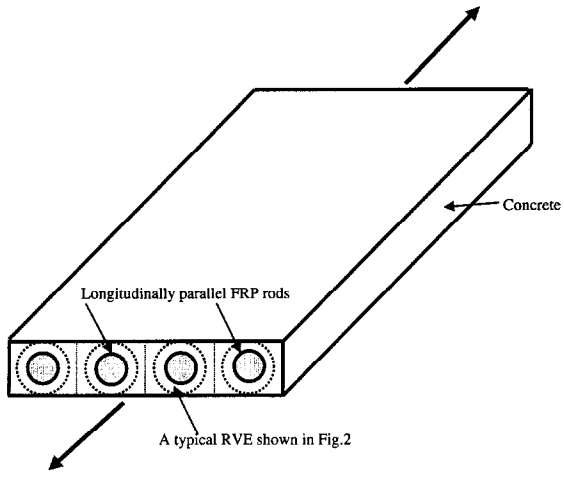

Fig. 3. Beam or plate reinforced with longitudinally parallel FRP rods under uniform tension.

$$\begin{Bmatrix} \sigma_r \\ \sigma_\theta \\ \sigma_z \\ \tau_{rz} \end{Bmatrix} = \begin{bmatrix} c_{11} & c_{12} & c_{13} & 0 \\ c_{12} & c_{11} & c_{13} & 0 \\ c_{13} & c_{13} & c_{33} & 0 \\ 0 & 0 & 0 & G_{rz} \end{bmatrix} \begin{Bmatrix} \varepsilon_r \\ \varepsilon_\theta \\ \varepsilon_z \\ \gamma_{rz} \end{Bmatrix} \tag{2}$$

and

$$\varepsilon_r = \frac{\partial u}{\partial r}, \quad \varepsilon_\theta = \frac{u}{r}, \quad \varepsilon_z = \frac{\partial w}{\partial z}, \quad \gamma_{rz} = \frac{\partial u}{\partial z} + \frac{\partial w}{\partial r}, \tag{3}$$

where u and w are respectively, the displacements in r and z directions. The $c_{ij}\,(i,j=1,2,3)$ are elastic stiffness constants. They can be expressed in terms of the material properties of the FRP rods, i.e., $c_{11} = E_T(1 - \nu_{LT}\nu_{TL})/Q$, $c_{12} = E_T(\nu_{TT} + \nu_{LT}\nu_{TL})/Q$, $c_{13} = E_T\nu_{LT}(1 + \nu_{TT})/Q$ and $c_{33} = E_L(1 - \nu_{TT}^2)/Q$, where $Q = 1 - \nu_{TT}^2 - 2\nu_{TL}\nu_{LT} - 2\nu_{TT}\nu_{TL}\nu_{LT}$ and $\nu_{LT}E_T = \nu_{TL}E_L$. Here E_L and E_T are respectively, Young's moduli in z- and r-directions and the $\nu_{ij}\,(i,j = T, L)$ are Poisson's ratios [16]. If the material is isotropic, $c_{11} = c_{33} = E(1-\nu)/((1+\nu)(1-2\nu))$, $c_{12} = c_{13} = \nu E/((1+\nu)(1-2\nu))$ and $G_{rz} = E/(2(1+\nu))$, where E is Young's modulus and ν the Poisson's ratio of the material.

Under generalized plane strain (if the dimension in z-direction of the RVE is large enough compared with the dimensions in other two directions), the classical Lamé solution is appropriate. The following linearly independent solutions are respectively found [14]:

$$u^f = D_{1f}\, r, \tag{4}$$

$$w^f = D_{3f} z \tag{5}$$

and

$$u^c = D_{1c} r + D_{2c}\frac{d^2}{4r}, \tag{6}$$

$$w^c = D_{3c} z, \tag{7}$$

where D_{1f}, D_{3f} and D_{ic} $(i = 1,2,3)$ are integral constants. The suffixes, f and c, denote FRP rods and concrete cover, respectively.

2.2. Splitting analysis

As mentioned in Section 1, splitting is one of the two failure modes that a FRP reinforced concrete may have. This happens particularly when lugged and sand particle coated FRP rods [4] are used as reinforcements since they may induce large circumferential forces in concrete. To the authors' best knowledge, there is no exact theoretical model so far to predict these forces. Tepfers [11] assumed that the radial component of bond stresses could be considered as hydrostatic pressure acting on the inner surface of the concrete cover (cylinder), and the concrete would crack if the induced circumferential stress reached its tensile capacity. Hence, when cracking occurs the concrete cover is further considered to be a cracked inner cylinder surrounding by an elastic outer one (Fig. 4). Under the assumptions, the following new features are introduced into the analysis in the paper. First, the anisotropic properties of the FRP rod and the deformation compatibility of the RVE in z-direction are included in the solution. Secondly, the Poisson's effect of cracked concrete and the compatibility of longitudinal strain at interfaces are considered.

The combined co-axial cylinder of Fig. 4 can be considered as a superimposition of the three parts shown in Fig. 5, i.e., (a) the elastic FRP rod; (b) the cracked part of concrete and; (c) the elastic part of concrete. To help the identification of the displacements and stresses in different parts of the concrete, two superscripts, 'i' and 'o', are used, respectively, to denote the cracked inner concrete cylinder and the elastic outer one.

Since parts (a) and (c) of the structure (Fig. 5) are elastic, their analyses can be carried out directly based on the solutions presented in Section 2.1. As a result, the relevant stress expressions for parts (a) and (c) are as follows:

For part (a)

$$\begin{Bmatrix} \sigma_r^f \\ \sigma_\theta^f \\ \sigma_z^f \end{Bmatrix} = \begin{bmatrix} c_{11} + c_{12} & c_{13} \\ c_{11} + c_{12} & c_{13} \\ 2c_{13} & c_{33} \end{bmatrix} \begin{Bmatrix} D_{1f} \\ D_{3f} \end{Bmatrix}, \tag{8}$$

For part (c)

$$\begin{Bmatrix} \sigma_r^o \\ \sigma_\theta^o \\ \sigma_z^o \end{Bmatrix} = E' \begin{Bmatrix} D_{1o} - (1-2\nu)D_{2o}\frac{d^2}{4r^2} + \nu D_{3o} \\ D_{1o} + (1-2\nu)D_{2o}\frac{d^2}{4r^2} + \nu D_{3o} \\ 2\nu D_{1o} + (1-\nu)D_{3o} \end{Bmatrix}, \tag{9}$$

where $E' = E/((1+\nu)(1-2\nu))$. The unknown coefficients D_{if} $(i = 1,3)$ and D_{jo} $(j = 1,2,3)$ will be determined by introducing boundary conditions and the continuity conditions at interfaces. However, this can

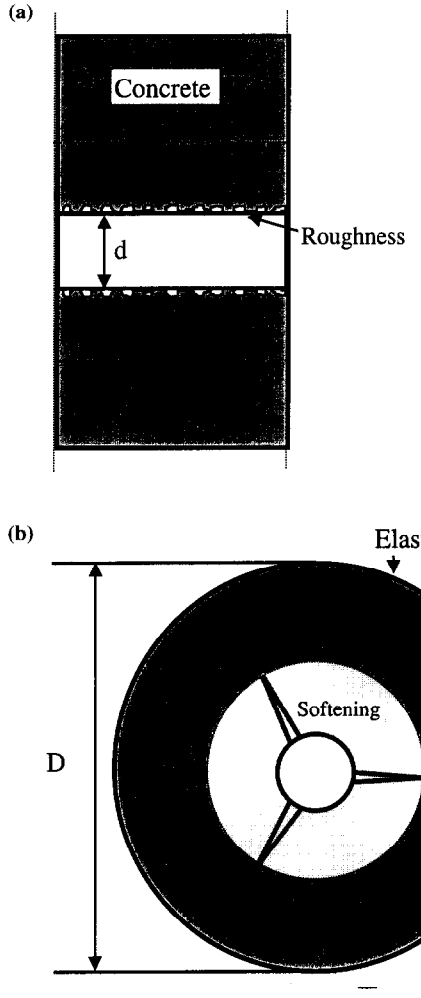

Fig. 4. Splitting failure of bond of FRP rod and surrounding concrete: (a) longitudinal section with roughness; and (b) cross section indicating material state.

only be done after considering the stress and displacement distributions of the cracked part, Fig. 5(b).

The stress analysis on the splitting part (b) in Fig. 5 is based on following assumptions:

(i) The total elongation in θ-direction (circumferential direction) in the cracked part is composed of n crack opening displacements (δ) and the elastic elongation is a constant [17] and equals $2\pi r_i \varepsilon_c$, where ε_c is the ultimate tensile strain of concrete, i.e.,

$$2\pi r_i \varepsilon_c = n\delta + 2\pi r \varepsilon_\theta^i. \tag{10}$$

Here ε_θ^i is the elastic strain in circumferential direction of the cracked part and is calculated by

$$\varepsilon_\theta^i = \frac{1}{E}[\sigma_\theta^i - v(\sigma_r^i + \sigma_z^i)]. \tag{11}$$

(ii) To consider the tension-softening property of the cracked concrete, an appropriate constitutive relation for circumferential stress, i.e., $\sigma_\theta^i(\delta)$, is assumed. In present analysis, the following displacement–stress constitutive relation for simple linear crack opening [10] is chosen.

$$\sigma_\theta^i = f_{ct}\left(1 - \frac{\delta}{\delta_c}\right), \tag{12}$$

where f_{ct} is the tensile strength of concrete; δ_c is the critical length that can be calculated from the tensile fracture energy of concrete [7,10].

(iii) A constant distribution of σ_z^i within the cracked part is further assumed based on stress distributions (8) and (9).

Substituting (11) into (10) and then taking derivation with respect to r yield

$$n\delta' + \frac{2\pi}{E}[r\sigma_\theta^i - v(r\sigma_r^i + r\sigma_z^i)]' = 0. \tag{13}$$

Substituting the derivation of Eq. (12) into (13) and considering assumption (iii), i.e., σ_z^i is a constant, one has

$$(r - r_c)(\sigma_\theta^i)' = v\sigma_z^i - (1 + v)\sigma_f^i, \tag{14}$$

where $r_c = nE\delta_c/(2\pi f_{ct})$. Integrating both sides of above equation and letting $\sigma_\theta^i|_{r=r_i} = f_{ct}$ at the interface give the circumferential stress in the cracked part,

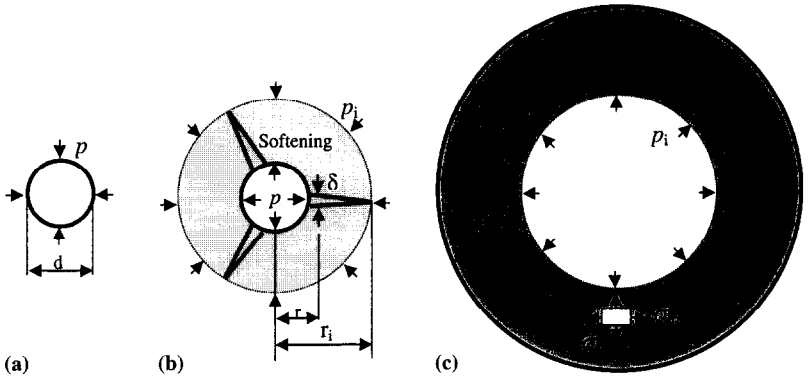

Fig. 5. Bond model for partly splitting of cracked FRP-concrete combined cylinder: (a) FRP rod; (b) cracked part of concrete; and (c) elastic part of concrete.

$$\sigma_\theta^{\mathrm{i}} = \frac{v}{1+v}\sigma_z^{\mathrm{i}} - \left(\frac{r_i - r_c}{r - r_c}\right)^{1+v}\left(\frac{v}{1+v}\sigma_z^{\mathrm{i}} - f_{\mathrm{ct}}\right). \tag{15}$$

Moreover, the equilibrium of the cracked part in r-direction gives

$$\sigma_r^{\mathrm{i}} r = p_i r_i - \int_r^{r_i} \sigma_\theta^{\mathrm{i}}\,\mathrm{d}r \quad (r_i \leqslant r \leqslant d/2). \tag{16}$$

From (15) and (16) the radial stress in the cracked concrete is

$$\sigma_r^{\mathrm{i}} = \frac{1}{r}\left\{p_i r_i - \frac{v}{1+v}\sigma_z^{\mathrm{i}}(r_i - r) - (r_i - r_c)\left[1 - \left(\frac{r_i - r_c}{r - r_c}\right)^{v}\right] \times \left(\frac{\sigma_z^{\mathrm{i}}}{1+v} - \frac{1}{v}f_{\mathrm{ct}}\right)\right\}. \tag{17}$$

To find the unknown constant, σ_z^{i}, in (15) and (17) and also the unknown coefficients D_{if} $(i = 1, 3)$ and D_{jo} $(j = 1, 2, 3)$ in (6)–(9), the following strain–stress relations of the cracked concrete are used so that all the displacements can be represented in terms of these unknown constants.

$$\varepsilon_r^{\mathrm{i}} = \frac{1}{E}(\sigma_r^{\mathrm{i}} - v\sigma_z^{\mathrm{i}}), \tag{18}$$

$$\varepsilon_z^{\mathrm{i}} = \frac{1}{E}(\sigma_z^{\mathrm{i}} - v\sigma_r^{\mathrm{i}}). \tag{19}$$

In above equations the effect of circumferential stress is ignored because of the presence of radial cracks. Inserting (15) and (17) into (18) and then integrating both sides of the equation from $r = d/2$ to $r = r_i$, one has

$$u^{\mathrm{i}}|_{r=r_i} - u^{\mathrm{i}}|_{r=d/2} = \frac{1}{E}\left\{\frac{v^2}{1+v}\left(\frac{d}{2} - r_i\right)\sigma_z^{\mathrm{i}} + \left(p_i - \frac{v}{1+v}\sigma_z^{\mathrm{i}}\right) r_i \ln\frac{2r_i}{d} - \left(\frac{\sigma_z^{\mathrm{i}}}{1+v} - \frac{1}{v}f_{\mathrm{ct}}\right)(r_i - r_c) \times \left[\ln\frac{2r_i}{d} - (r_i - r_c)^{v}\int_{d/2}^{r_i}\frac{\mathrm{d}r}{r(r - r_c)^{v}}\right]\right\}. \tag{20}$$

Based on the stresses and displacements of all the three parts of the combined cylinder, final solutions can be found after introducing boundary conditions and the continuity conditions at interfaces.

2.3. Boundary conditions

The continuity conditions of stresses and displacements at interfaces between the cracked part and the two adjacent parts in the RVE (Fig. 4) can be represented by Eqs. (21)–(25) shown below.

Because of the continuity of radial displacements at the interfaces of different parts of the concrete, the left-hand side of (20) can be written as

$$u^{\mathrm{o}}|_{r=r_i} - u^{f}|_{r=d/2} = D_{1o} r_i + D_{2o}\frac{d^2}{4r_i} - D_{1f}\frac{d}{2}. \tag{21}$$

The compatibility of the longitudinal displacements/strains at interfaces requires

$$\varepsilon_z^{\mathrm{i}}|_{r=d/2} = D_{3f} \tag{22}$$

and

$$\varepsilon_z^{\mathrm{i}}|_{r=r_i} = D_{3o}. \tag{23}$$

The continuity conditions of radial stresses at $r = d/2$ and $r = r_i$ give

$$\sigma_r^{f}|_{r=d/2} = \sigma_r^{\mathrm{i}}|_{r=d/2}, \tag{24}$$

$$\sigma_r^{\mathrm{o}}|_{r=r_i} = \sigma_r^{\mathrm{i}}|_{r=r_i} = p_i. \tag{25}$$

As a criteria for crack development at $r = r_i$, the circumferential stress of concrete must satisfy

$$\sigma_\theta^{\mathrm{o}}|_{r=r_i} = f_{\mathrm{ct}}. \tag{26}$$

The outer surface conditions of the cylinder can be represented by either

$$u^{\mathrm{o}}|_{r=D/2} = u_o \tag{27}$$

or

$$\sigma_r^{\mathrm{o}}|_{r=D/2} = \sigma_o \tag{28}$$

depending on how the RVE is specified. u_o and σ_o here reflect the interactions between the RVE and its surrounding materials and can be determined on the basis of either the test results of carefully designed experiments or an empirical selection of appropriate numerical simulations.

After substituting (20) into (21), (19) into (22) and (23), (8) and (17) into (24) and (9) into (26), respectively, Eqs. (21)–(26), together with (27) or (28), give a set of linear equations from which the unknown constants, D_{if} $(i = 1, 3)$, D_{jo} $(j = 1, 2, 3)$, σ_z^{i} and p_i, can be solved. For example, for a given displacement at the outer surface of the cylinder (27), the solutions are as follows:

$$\mathbf{A}\{\mathbf{D}\} = \{\mathbf{F}\}, \tag{29}$$

where

$$\{\mathbf{D}\} = \left[D_{1f} \quad D_{3f} \quad D_{1o} \quad D_{2o} \quad D_{3o} \quad \sigma_z^{\mathrm{i}}/f_{\mathrm{ct}} \quad p_i/f_{\mathrm{ct}}\right]^{\mathrm{T}},$$

$$\{\mathbf{F}\} = [F_1 \quad F_2 \quad F_3 \quad (1+v)(1-2v)\varepsilon_c \quad (1+v)\varepsilon_c \quad 0 \quad 2u_o/D]^{\mathrm{T}} \tag{30}$$

and the matrix

$$\mathbf{A} = \begin{bmatrix} 1 & 0 & -\frac{2r_i}{d} & -\frac{d}{2r_i} & 0 & A_{16} & \varepsilon_c \frac{2r_i}{d} \ln \frac{2r_i}{d} \\ 0 & -1 & 0 & 0 & 0 & A_{26} & -v\varepsilon_c \frac{2r_i}{d} \\ \frac{c_{11}+c_{12}}{E} & \frac{c_{13}}{E} & 0 & 0 & 0 & A_{36} & -\varepsilon_c \frac{2r_i}{d} \\ 0 & 0 & 2 & 0 & 2v & 0 & -(1+v)(1-2v)\varepsilon_c \\ 0 & 0 & 0 & \frac{d^2}{2r_i^2} & 0 & 0 & (1+v)\varepsilon_c \\ 0 & 0 & 0 & 0 & 1 & -\varepsilon_c & v\varepsilon_c \\ 0 & 0 & 1 & \frac{d^2}{D^2} & 0 & 0 & 0 \end{bmatrix}. \tag{31}$$

In Eqs. (30) and (31),

$$F_1 = -\frac{2\varepsilon_c}{v}\frac{r_i - r_c}{d}\left[\ln\frac{2r_i}{d} - \int_1^{2r_i/d}\left(\frac{r_i/d - r_c/d}{r/2 - r_c/d}\right)^v \frac{\mathrm{d}r}{r}\right],$$

$$F_2 = \frac{2\varepsilon_c(r_i - r_c)}{d}\left[1 - \left(\frac{r_i - r_c}{d/2 - r_c}\right)^v\right],$$

$$F_3 = \frac{2\varepsilon_c}{v}\frac{r_i - r_c}{d}\left[1 - \left(\frac{r_i - r_c}{d/2 - r_c}\right)^v\right],$$

$$A_{16} = \frac{v\varepsilon_c}{1+v}\left[v\left(1 - \frac{2r_i}{d}\right) - \frac{2r_i}{d}\ln\frac{2r_i}{d}\right] + \frac{v}{1+v}F_1,$$

$$A_{26} = \varepsilon_c\left[1 + \frac{v^2}{1+v}\left(\frac{2r_i}{d} - 1\right)\right] + \frac{v}{1+v}F_2,$$

$$A_{36} = \frac{v\varepsilon_c}{1+v}\left(\frac{2r_i}{d} - 1\right) + \frac{v}{1+v}F_3$$

and $\varepsilon_c = f_{ct}/E$ is the tensile fracture strain of the concrete. If the boundary condition on the outer surface is given by (28), Eq. (29) can still be used except that the last element in Eq. (30) and the last row in matrix (31) become σ_o/E' and $[0\ 0\ 1\ -(1-2v)d^2/D^2\ v\ 0\ 0]$, respectively.

Once $\{\mathbf{D}\}$ is known, all stresses can be determined. The pressure p on the FRP rod for a given crack radius in concrete can then be obtained. The corresponding loads acting on the ends of the RVE can also be calculated.

3. Numerical results and discussions

Consider a combined cylinder with $D = 80$ mm and $d = 16$ mm (Fig. 4). The material constants of FRP rod are shown in Table 1 and the material properties of concrete are given [10] by $f_{ct} = 4$ MPa, $E = 30$ GPa and $\delta_c = 0.0725$ mm. The Poisson's ratio of the concrete is assumed to be 0.15. The numerical calculation is carried out only for the cylinder having the outer surface condition (28) specified by

$$\sigma_r^o|_{r=D/2} = 0. \tag{32}$$

In the calculation, the number and the length of the cracks in the concrete are used as parameters, against which stress distributions are shown in Figs. 6–13.

Fig. 6 shows the changes of the internal pressure on the inner surface of the cracked concrete (Fig. 5) against crack radius. The results shown are for concrete having different number of cracks ($n = 1$, 2 and 4) and no Poisson's effect in the cracked part of concrete. The FEM results shown in these figures for comparisons are from Olofsson et al. [10]. In fact, letting $v = 0$ in (15) and (17), the special forms of the solution for cracked concrete are identical to the ones given by Olofsson et al. [10], i.e.,

Table 1
Engineering constants of FRP rod (T300 Graphite)

E_L (GPa)	E_T (GPa)	ν_{LT}	ν_{TT}	G_{rz} (GPa)
226	22	0.30	0.42	4.83

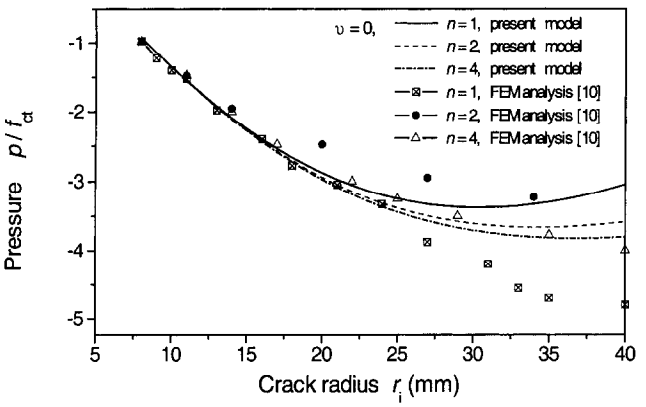

Fig. 6. Variation of internal pressure p against crack radius ($v = 0$).

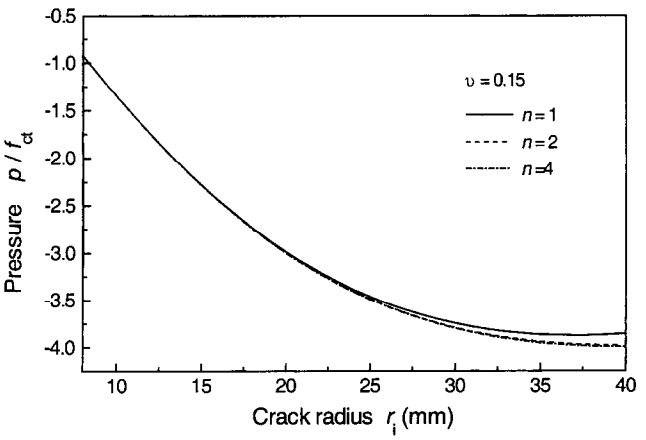

Fig. 7. Variation of internal pressure p against crack radius for different crack number ($v = 0.15$).

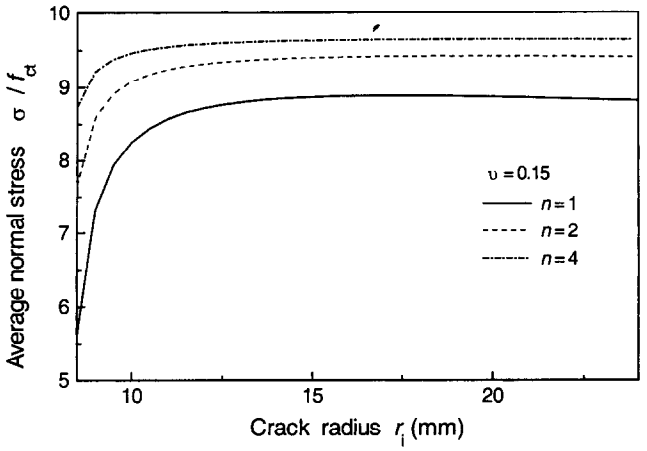

Fig. 8. Variation of average normal stress σ against crack radius ($v = 0.15$).

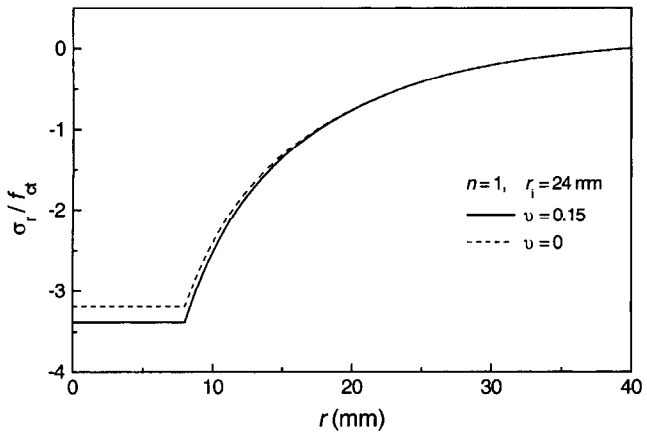

Fig. 9. Variation of σ_r along r-direction of the cylinder with and without Poisson's effect.

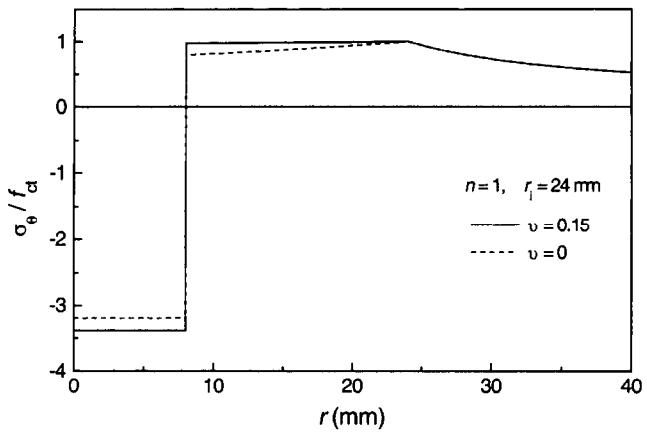

Fig. 10. Variation of circumferential stress σ_θ along r-direction of the cylinder with and without Poission's effect.

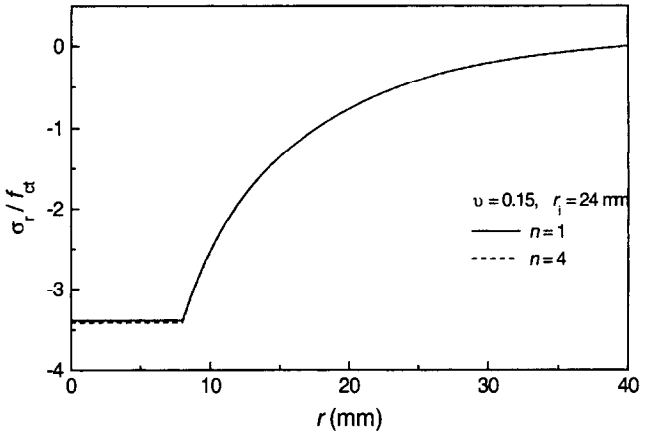

Fig. 11. Influence of crack number on σ_r along r-direction of the cylinder ($v = 0.15$).

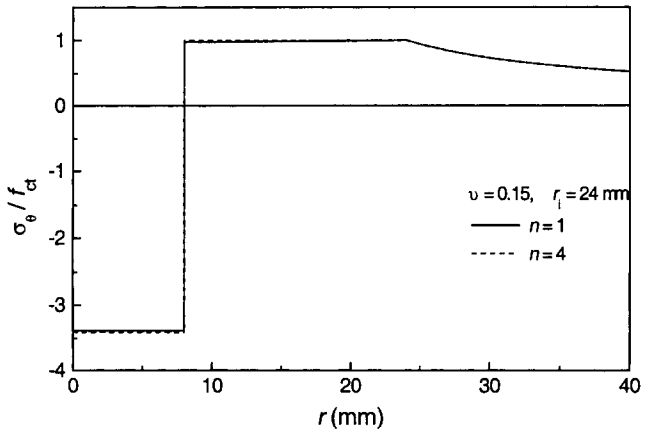

Fig. 12. Influence of crack number on circumferential stress σ_θ along r-direction of the cylinder ($v = 0.15$).

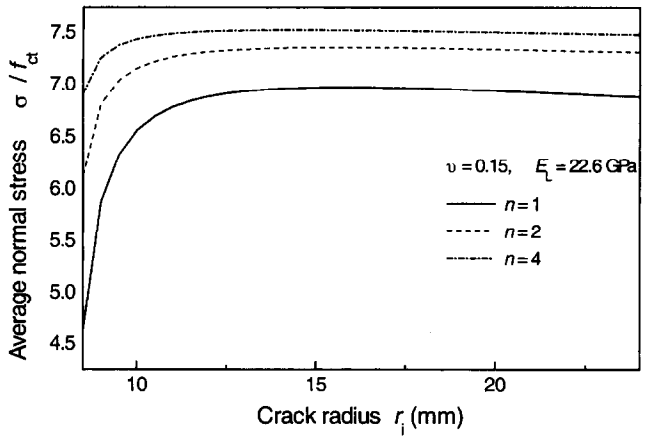

Fig. 13. The effect of longitudinal modulus of FRP rod on the variation of average normal stress σ ($v = 0.15$).

$$\sigma_\theta^{\mathrm{i}} = \frac{r_i - r_c}{r - r_c} f_{\mathrm{ct}}, \tag{33}$$

$$\sigma_r^{\mathrm{i}} = \frac{r_i}{r} p_i + f_{\mathrm{ct}} \frac{(r_i - r_c)}{r} \ln \frac{r - r_c}{r_i - r_c}. \tag{34}$$

Consequently, Eqs. (18)–(20) for this special case should also be changed accordingly. It is seen that the agreement between present results and the FEM ones is good for small crack radius but less satisfactory in general when crack radius is large, particularly for $n=1$. Olofsson et al. attributed such a disagreement to the purely academic nature of the splitting case and considered two more 'likely' cases $n=2$ and $n=4$. The authors believe that one of the main reasons for this disagreement is that the effect of Poisson's ratio and the compatibility of the longitudinal displacement at interface are not considered, which obviously affects the calculation of the internal pressure p (see the comparison of Eqs. (17) and (34)) especially when the crack number is small. It has been observed that after considering the effect of Poisson's ratio, the influence of the crack number on the internal pressure p is reduced. Fig. 7 is the calculated results of the internal pressure p after considering Poisson's ratio of the cracked part. It can be seen that although the internal pressure increases as the number of cracks increases, the differences in internal pressure are not significant.

For given crack lengths, Fig. 8 shows the average normal stresses on the ends of the RVE with the effect of Poisson's ratio being considered. The average normal stress is defined by

$$2\int_0^{d/2} \sigma_z^f r\,\mathrm{d}r + 2\int_{d/2}^{r_i} \sigma_z^{\mathrm{i}} r\,\mathrm{d}r + 2\int_{r_i}^{D/2} \sigma_z^{\mathrm{o}} r\,\mathrm{d}r = \frac{D^2}{4}\sigma. \tag{35}$$

The applied average tensile stress varies smoothly as the growth of the crack radius. It can be observed that in general a larger applied force induces more cracks. This is because that, as σ increases, the circumferential stress σ_θ will increase. When σ_θ reaches the concrete strength, more cracks will be induced due to the stress redistribution on the basis of the softening model (12).

Figs. 9 and 10 show the distributions of σ_r and σ_θ on the cross-section of the cylinder when the crack radius r_i is 24 mm and the crack number is one. The influence of Poisson's ratio is observed. It can be seen that considering Poisson's ratio results in larger σ_r and σ_θ in both FRP rod and the cracked part of concrete. The fact that neglecting Poisson's ratio may produce less safe design should be noticed in the safety assessment of such FRP/concrete hybrid structures.

Figs. 11 and 12 show the distributions of σ_r and σ_θ across the cross-section of the cylinder with $v=0.15$ and $r_i=24$ mm for different numbers of cracks. The comparisons are made between the results for $n=1$ and $n=4$. Obviously, the influence of the crack number n is very small.

Fig. 13 presents results for the cylinder reinforced with a FRP rod having different elastic constants. The longitudinal elastic modulus E_{L} used here is 10 times smaller than the one used previously. Comparing Fig. 13 with Fig. 8, the average normal stress σ is decreased by up to 25% depending on the length of cracks. It is also observed that the change of E_{L} has very small effects on the distributions of σ_r and σ_θ (for which corresponding results are not presented). Since the internal pressure p is the main concern in splitting analysis, it may be concluded that unlike pull-out failure, the anisotropic property of FRP reinforcement is not considered as a dominating factor in characterizing the splitting failure.

4. Conclusions

A modified theoretical model for the splitting analysis of FRP/concrete hybrid elements has been established in the paper. The new model enables Poisson's effect and strain compatibility in longitudinal direction be included in the analysis.

Numerical results were obtained and compared with those from the simple model [10] where Poisson's ratio of cracked concrete and compatibility in longitudinal direction of a RVE were ignored. It was observed that neglecting Poisson's ratio of cracked concrete may yield an underestimation of radial and circumferential stresses and the material properties of FRP reinforcement play an insignificant role in splitting failure of FRP/concrete hybrid structures.

Acknowledgements

The authors would like to acknowledge the support of EPSRC (Grant No. GR/L91450). The authors also wish to thank Prof. J.G. Cabrera for his invaluable support during the course of this research.

References

[1] Clarke JL. Non-ferrous reinforcement. Mag Concr Res 1998;50(1):1–3.
[2] Cosenza E, Manfredi G, Realfonzo R. Behavior and modeling of bond of FRP rebars to concrete. J Compos Construction 1997;1(2):40–51.
[3] Ei-Brdry MM, editor. Advanced composite materials in bridges and structures. Montréal, Canada: Canadian Society of Civil Engineers, 1996.

[4] Bakis CE, Uppuluri VS, Nanni A, Boothby TE. Analysis of bonding mechanisms of smooth and lugged FRP rods embedded in concrete. Comp Sci and Technol 1998;58:1307–19.
[5] Nanni A, Bakis CE, Boothby TE. Test methods for FRP-concrete systems subjected to mechanical loads: state-of-the-art review. J Reinf Plastics and Composites 1995;14:524–58.
[6] Benmokrane B, Tighiouart B, Chaallal O. Bond strength and load distribution of composite GFRP reinforcing bars in concrete. ACI Mater J 1996;93:246–53.
[7] Karihaloo BL. Tension softening diagrams and longitudinally reinforced beam. In: Baker G, Karihaloo BL, editors. Fracture of Brittle, Disordered Materials – Concrete, Rock and Ceramics. UK: E&FN Son, Chapman & Hall, 1995. p. 35–50.
[8] Noghabai K. Effect of tension softening on the performance of concrete structures. Doctoral Thesis, Luleå University of Technology, Sweden, 1998:150 pp.
[9] Wu ZJ, Ye JQ, Cabrera JG. 3D Analysis of stress transfer in the micro-mechanics of fiber reinforced composites by using an eigenfunction expansion method. J Mech Phys Solids 2000;48(5):1037–63.
[10] Olofsson T, Noghabai K, Ohlsson U, Elfgren L. Anchorage and bond properties in concrete. In: Baker G, Karihaloo BL, editors. Fracture of Brittle, Disordered Materials – Concrete, Rock and Ceramics. UK: E&FN Son, Chapman & Hall, 1995. p. 525–43.
[11] Tepfers R. Cracking of concrete cover along anchored deformed reinforcing bars. Mag Concr Res 1979;31:3–12.
[12] Cornelius Van der Veen. Cryogenic bond stress-slip relationship. Doctoral Thesis, Delft University of Technology, The Netherlands, 1990:111 pp.
[13] Wu ZJ. An investigation on the interface of fiber reinforced composite – theory and experiment. Ph.D. Dissertation of Shanghai Jiao Tong University, Shanghai, 1991.
[14] Smith GE, Spencer AJM. Interfacial tractions in a fibre-reinforced elastic composite material. J Mech Phys Solids 1970;18:81–100.
[15] McCartney LN. New theoretical model of stress transfer between fibre and matrix in a uniaxially fibre-reinforced composite. Proc Roy Soc Lond A 1989;425:215–44.
[16] Jones RM. Mechanics of composite materials, 2nd ed. Philadelphia, PA: Taylor & Francis, 1999.
[17] Reinhardt HW. Bond of steel to strain-softening concrete taking account of loading rate. In: Bazant ZP, editor. Fracture Mechanics of Concrete Structures. London: Elsevier Applied Science, 1992. p. 809–20.